Available online at www.sciencedirect.com
ScienceDirect
Journal of Crystal Growth 308 (2007) 141–150
JOURNAL OF CRYSTAL GROWTH
www.elsevier.com/locate/jcrysgro

Face-by-face growth of sucrose crystals from aqueous solutions in the presence of raffinose—II: Growth morphology and segregation

G. Sgualdino[a], D. Aquilano[b,*], L. Pastero[b], G. Vaccari[a]

[a]*Dipartimento di Chimica, Università, via L. Borsari, 46-44100 Ferrara, Italy*
[b]*Dipartimento di Scienze Mineralogiche e Petrologiche, Università, via Valperga Caluso, 35-10125 Torino, Italy*

Received 20 March 2007; received in revised form 28 July 2007; accepted 6 August 2007
Communicated by R. Kern
Available online 11 August 2007

Abstract

Raffinose segregation into sucrose crystals is experimentally determined along with the modifications of the quantitative sucrose growth morphology, which are in turn related to the different growth conditions. (C_{raff}, σ) morphodromes nicely represent the conflict between the supersaturation and the raffinose concentration in the solution on the growth morphology, while the overall segregation rate is nearly proportional to the linear overall crystal growth rate. Chernov and Burton–Prim–Slichter models, checked to fit our k_{eff} and $\ln(k_{eff}^{-1}-1)$ coefficients as a function of the supersaturation and of the mean linear overall growth rate, do not allow to know whether the segregation occurs either by a process dominated by surface integration, or by additive transfer dominated by volume diffusion within the boundary layer. The distribution of segregated raffinose strictly depends on the $\{h\,k\,l\}$ growth sectors and doped crystals contain deformed lattice zones, as it comes out from X-ray powder diagrams.

PACS: 81.10.Aj; 81.10.Dn

Keywords: A1. Crystal morphology; A1. Impurity absorption; A2. Growth from solutions; B1. Sucrose

1. Introduction

The most common morphology of sucrose crystals (α-D-glucopyranosyl-(1→2)-β-D-fructofuranoside; space group $P2_1$) grown from pure aqueous solutions shows seven or eight forms (Fig. 1). In the first part of this work [1], concerning the sucrose crystallization in the presence of raffinose (α-D-galactopyranosyl-1-(1→6)-α-D-glucopyranosyl-(1→2)-β-D-fructofuranoside), we dealt with both the growth kinetics and the surface adsorption mechanisms, at 40 °C, of the four main flat (F) forms, i.e., the non-polar $\{1\,0\,0\}$, $\{1\,0\,\bar{1}\}$ and the polar ones $\{1\,1\,0\}$ and $\{\bar{1}\,\bar{1}\,0\}$, and showed that

(i) raffinose dramatically slows down the growth rate of $\{1\,1\,0\}$, $\{1\,0\,\bar{1}\}$ and $\{1\,0\,0\}$ forms and gives rise to *dead zones* on the growth isotherms, without modifying yet the spiral growth mechanism;
(ii) raffinose works as a *blocker tailor-made additive* on the first two forms, due to the stockades of galactose rings emerging from the affected surfaces, while the sucrose moiety is adsorbed;
(iii) kinks are the prevailing adsorption sites, as proved by the good fit of our kinetic data to the Kubota–Mullin model, associated to Langmuir-type isotherms [2];
(iv) $\{1\,0\,0\}$ mimes the kinetic behaviour of the $\{1\,1\,0\}$ and $\{1\,0\,\bar{1}\}$ forms, due to the peculiar structure of its surface;
(v) the $\{\bar{1}\,\bar{1}\,0\}$ form is weakly affected, at least up to raffinose concentration $C_{raff} \approx 3.0\%$ and 1.0% H_2O, at supersaturation $\sigma = 0.080$ and 0.040, respectively, because of the low structural compatibility between raffinose molecules and kink sites of this form.

*Corresponding author. Tel.: +39 011 6705125; fax: +39 011 6705128.
E-mail address: dino.aquilano@unito.it (D. Aquilano).

0022-0248/$ - see front matter © 2007 Elsevier B.V. All rights reserved.
doi:10.1016/j.jcrysgro.2007.08.003

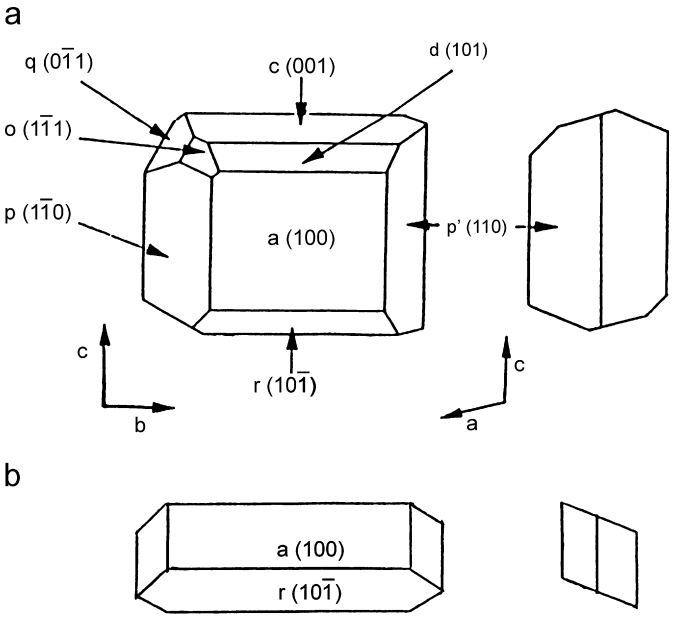

Fig. 1. Common growth morphologies of sucrose crystals: (a) in pure solution and (b) in the presence of medium/high raffinose concentrations in solution (C_{raff}).

To have a more comprehensive outline on the raffinose effects, it still remained to be investigated both its incorporation inside the sucrose crystals and the modifications of the growth morphology which is strictly related to the impact of the additive upon the kinetics of each $\{h\,k\,l\}$ form. The impact changing from face to face, different crystal morphologies can result. Besides, strongly bonded additives are incorporated into the crystal lattice so giving rise to the absorption process. This can lead to lattice strains altering the bulk properties of the crystal, which in turn affect both its kinetics and quality.

The incorporation ability of a crystal is described by the distribution coefficient, defined as the ratio of the additive concentration in the crystal and in the mother phase, at equilibrium. However, the absorption is not an equilibrium process, the distribution coefficient being not constant over a wide range of solution compositions; moreover, the impurity amounts may differ in the various growth sectors of the host crystal, according to the absorption ability of the surfaces of the corresponding forms. Hence, the thermodynamic analysis of the additive partitioning cannot account for the actual distribution coefficient value, which is strongly influenced not only by the experimental conditions but also by the crystallographic orientations [3]. To emphasize the non-uniformity of the absorption process it is customary to speak in terms of segregation process, described by means of the effective segregation coefficient k_{eff}:

$$k_{eff} = \frac{C_{raff}^{cryst/sol}}{C_{raff}^{sol}} \approx \frac{C_{raff}^{cryst}}{C_{raff}^{sol}}, \tag{1}$$

where $C_{raff}^{cryst/sol}$, C_{raff}^{sol}, C_{raff}^{cryst} are the additive concentration at the crystal/solution interface, in the solution bulk and in the crystal, respectively. Concentrations are expressed in grams of additive per grams of component of the host crystal. Because the solute diffusion inside the crystals is negligible within the growth time, we can assume $C_{raff}^{cryst} \approx C_{raff}^{cryst/sol}$ for steady growth (boundary layer approximation).

Raffinose contents in doped sucrose crystals were determined and distribution coefficients sometimes calculated [4,5]. However, no attempts were made to investigate the dependence of k_{eff} on controlled growth conditions. This topic is faced in the present paper, which deals with the raffinose segregation into the sucrose crystals along with the modifications of the growth morphology and their correlations under different growth conditions.

2. Experimental procedure

The isothermal growth ($40 \pm 0.05\,^{\circ}C$) of doped and undoped sucrose crystals, at different σ and C_{raff} values, is described in detail in the first part of this work [1]. Let us only remember that the experiments were carried out on statistical populations of 12 single crystals (seed size $= 0.8 \pm 0.2$ mg) supported by a frame rotating (at 10 rpm) inside a 500 ml cylindrical vessel equipped with a water jacket. Supersaturation $0.020 \leqslant \sigma \leqslant 0.080$ and raffinose concentration ($0.0 \leqslant C_{raff} \leqslant 8.0\%$ H_2O) ranges were explored. Moreover, a second set of experiments was carried on bigger seeds (6.8 ± 0.4 mg) at $\sigma = 0.080$ and variable C_{raff}. To draw the steady growth morphologies, the advancement rates of the two $\{0\,0\,1\}$ and $\{1\,0\,\bar{1}\}$ nonpolar forms are here considered, along with those of the aforementioned forms for the studies on kinetics and absorption. The normal growth rates R_{hkl} and the axial ratios on each run were measured *ex situ* from the displacements of couples of faces (or edges) of single crystals under an optical microscope at magnifications of $50\times$ or $25\times$.

Besides, both seeds and grown crystals were weighted to calculate the *overall mass growth rates*:

$$R_G = \frac{1}{A_T}\frac{\Delta m}{\Delta t}, \tag{2}$$

where A_T is the total surface area of the crystals and Δm their mass increase during the growth time Δt. Balances having reciprocal sensitivity on the order of 10^{-2} mg per division were used.

The raffinose concentration inside the doped crystals was analysed by means of a home-made TLC set up. One or more doped crystals (roughly 40–50 mg) were dissolved into 5 ml of water–acetone (1:1 v/v) solution. Diol plates, buffered with a 0.05 M solution of sodium acetate, were used as a stationary phase and a mixture of acetonitrile–acetone–water (40:40:20) as ternary eluent. Spots of samples and standards for the calibration were applied on the same 20×10 diol plate (Merk) by means of a semiautomatic sample application device CAMAG Linomat 5. Isocratic

elution was carried out in twin-trough chambers without pre-saturation, with 20 min overrunning. After elution, the plates were dried and placed again in the chamber in the presence of vapours of 12 N HCl for 30 min, to improve the sensitivity of the developer. The plates were derivatized with 4-amino-benzoic acid; then, the chromatograms were scanned using a densitometer (absorbance at $\lambda_{max} = 460$ nm, TLC Scanner 3-Camag interfaced with a computer and managed by winCATS 1.2.6 software). The C_{raff} variation inside the crystals of the same growth run was estimated analysing thrice three crystals. The variation coefficient, depending both on analytic errors and on fluctuations in the segregation process, was lower than 10%.

X-ray powder diffraction patterns (XRPD) of the doped crystals were carried out by a diffractometer *Siemens 5000*, in order to investigate the lattice strains due to the segregated raffinose. The patterns were processed by decomposing the peak profiles into Gauss or Voigt's symmetrical functions with the aid of the profile-fitting software *Diffrac-AT (Socabim)*.

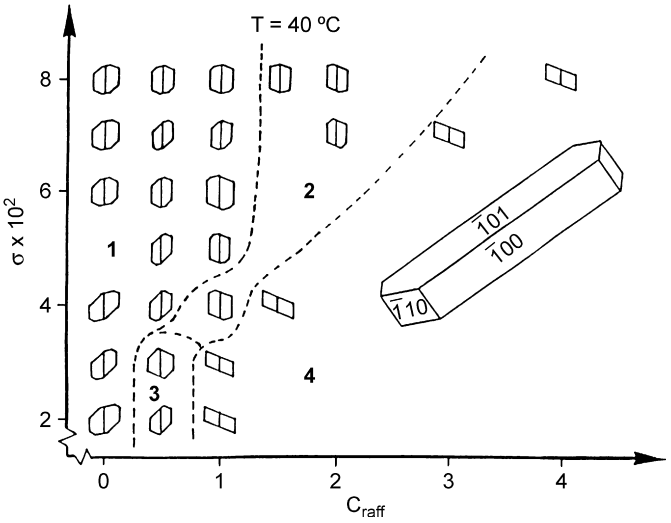

Fig. 2. Morphodrome showing the morphological changes of sucrose crystals in dependence of σ and C_{raff}. Dotted lines define the domains of the following morphologies: (1) complete; (2) reduced, that is without the {1 0 1} or {0 0 1} forms (3) in the {h 0 l} zone; and (4) simple.

3. Results

3.1. Growth morphology

In pure solution, increasing σ promoted more isometric crystals bounded by seven main forms. As much as C_{raff} increases, crystals became more and more elongated along [0 1 0] direction, while the {1 0 1} and {0 0 1} forms progressively disappear from the growth morphology, their kinetics being less affected with respect to those of the other iso-zonal forms (Fig. 1). The simplest crystal shape included four forms only, i.e., {1 0 0}, {1 0 $\bar{1}$}, {1 1 0} and {$\bar{1}$ $\bar{1}$ 0}. The {$\bar{1}$ $\bar{1}$ 0} form, which is only weakly affected by raffinose, can survive because it is not in competition with any other important form [1,6,7]. All these effects did not depend on the seed size.

The asymmetric evolution of the crystal morphologies were quantitatively estimated by means of the ratios:

$$\varepsilon = \frac{a'}{b}, \qquad \delta = \frac{c}{b}, \tag{3}$$

where b and c are the crystal lengths along the [0 1 0] and [0 0 1] directions, respectively, while a' represents the distance between the faces of the {1 0 0} pinacoid [1] (Fig. 1). Both ε and δ values depended on several parameters as T, σ, nature and concentration of impurities. Their dependence on C_{raff} was quite different: ε values were nearly constant up to $C_{raff} \approx 3\%$ or 1% H_2O at $\sigma = 0.080$ or 0.040, respectively, but over this value they decreased monotonically. On the contrary, the curves (δ vs C_{raff}) exhibited a maximum before decreasing (Fig. 3a and b).

The growth shapes of the crystals, acquired under very long steady growth runs, were predicted by applying the Wulff's rule to the growth polyhedra [8] at different σ and C_{raff} values. To do that the R_{hkl} values were used as input central distances of the {h k l} forms in the software SHAPE 6.0.1 [9]. The calculated growth shapes [7] were collected in a morphodrome giving an overall view on the morphological changes due to both σ and C_{raff} (Fig. 2). Indeed, the theoretical ε and δ ratios were obtained from the steady growth shapes. Experimental and theoretical values of ε and δ agreed only within the low additive concentration range (Figs. 3a,b and 4).

3.2. Overall kinetics

Till now, we dealt with the face-by-face growth rates for both kinetic and morphological considerations. However, the models describing the solution/crystal transfer of an additive, need the knowledge of the mean linear overall growth rates of the crystals, defined as

$$G = 0.5\left(\frac{dL_c}{dt}\right), \tag{4}$$

where L_c is a characteristic linear size of crystals evaluated on large crystal population by means of image or sieve analysis. For sucrose L_c is expressed by [10]

$$L_c = (b^2 c)^{1/3}. \tag{5}$$

However, we were in doubt as to whether relationship (5) can hold for our small samples too. Then, we calculated G in two other independent ways, both involving mass variations and matched the values.

In the first way, we applied the well-known relationship between the overall mass growth rate (Eq. (1)) and the overall linear growth rate G [11]:

$$R_G = \left(6\rho_c \frac{\alpha}{\beta}\right) G, \tag{6}$$

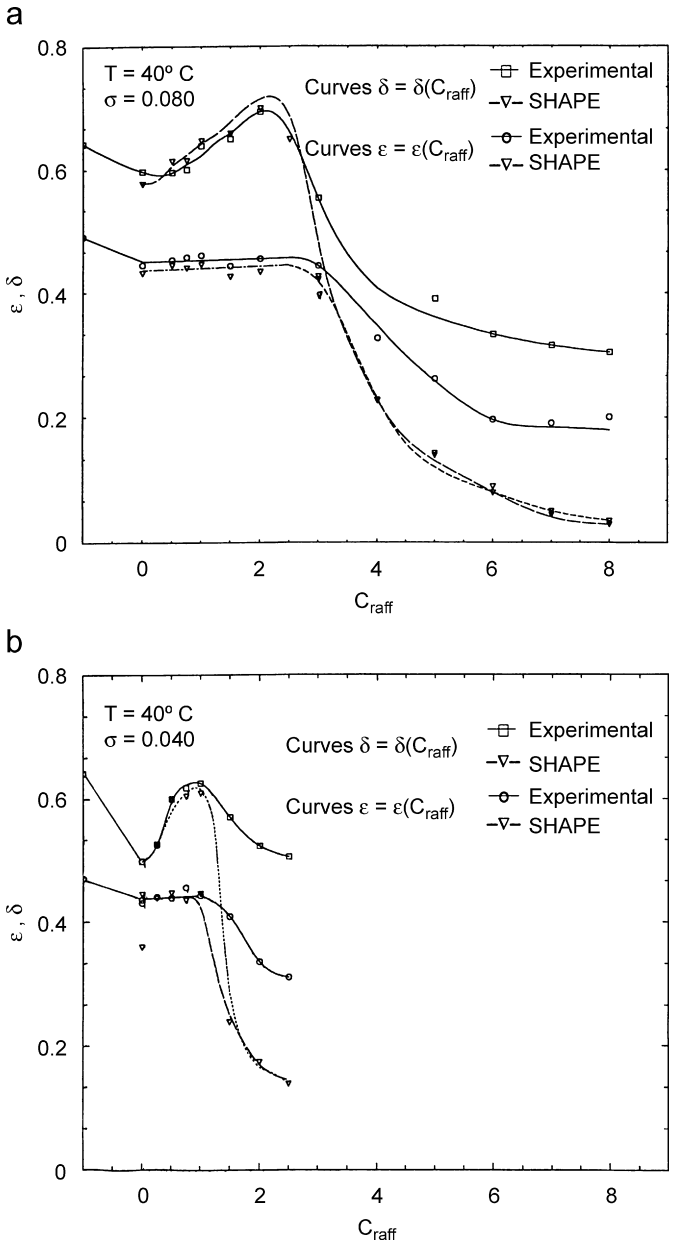

Fig. 3. Quantitative morphology, that is experimental and theoretical ε and δ ratios for sucrose crystals, as a function of C_{raff}: (a) at $\sigma = 0.040$ and (b) at $\sigma = 0.080$.

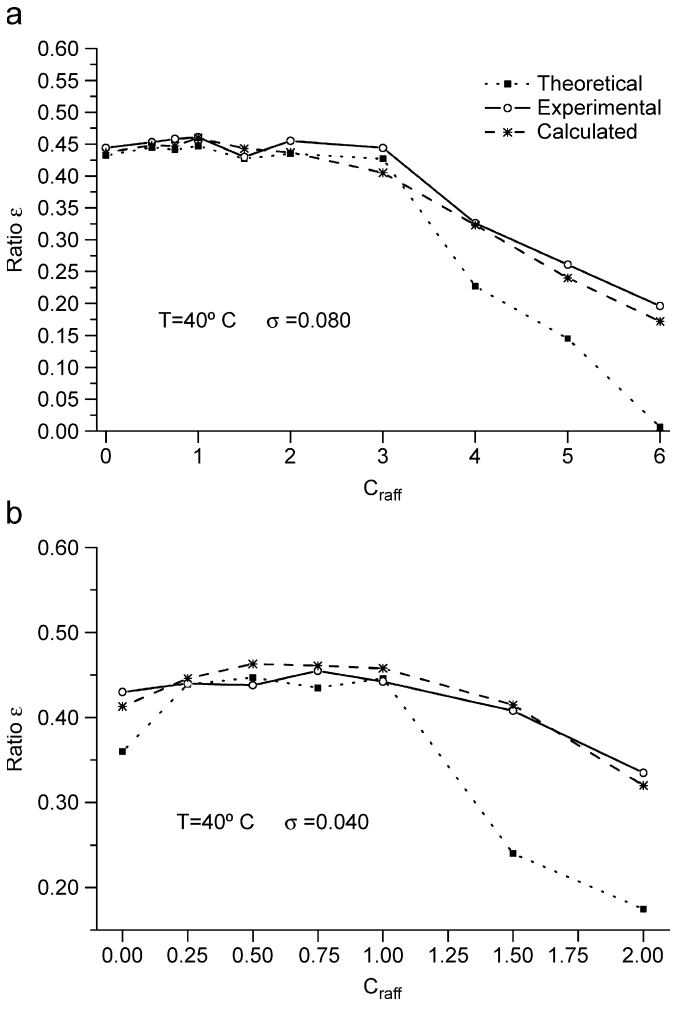

Fig. 4. Comparison between experimental and theoretical ε and δ ratios with those calculated according to the formula (19).

where ρ_c is the crystal density, while α and β are the volume and the surface shape factor, respectively, defined by

$$\alpha = \frac{m_c}{\rho_c L_c^3}, \qquad \beta = \frac{A_c}{L_c^2}, \tag{7}$$

where m_c and A_c being the averaged mass and surface area of the crystals, respectively. We cannot integrate Eq. (2) because the total surface area increase during a run cannot be neglected. Then, we calculated the mean value A_T based on the initial and final areas as [11]

$$A_T = \left(\frac{1}{3}\right) A_s \left[1 + \left(\frac{m_c}{m_s}\right)^{1/3} + \left(\frac{m_c}{m_s}\right)^{2/3}\right], \tag{8}$$

where m_s and m_c being the total mass of seeds and crystals, respectively. A_s is given by

$$A_s = \beta(\rho\alpha)^{-2/3} m_s^{2/3} = F m_s^{2/3}, \tag{9}$$

where F is the crystal shape factor. Finally, G was evaluated as [11]

$$G = \frac{m_c^{1/3} - m_s^{1/3}}{2(\alpha\rho N)^{1/3} t}, \tag{10}$$

where N is the number of crystals in a run.

The correlation straights lines in Fig. 5 indicate that the G values, evaluated by the three independent ways, match within a 95% confidence interval. Therefore, the validity of relationship (5) was verified. We choose the shape factor values proposed by Bubník and Kadlec [10], $\alpha = 0.307$, $\beta = 2.767$, $F = 4.47\,\mathrm{mm^2\,mg^{-2/3}}$ and $\rho_c = 1.587 \times 10^{-3}\,\mathrm{g\,mm^{-3}}$, from a check on 200 seeds. All parameters were considered to be constant, even if this assumption can be questionable for α and β, at low σ and high C_{raff} values. On the other hand, density changes of doped crystals were

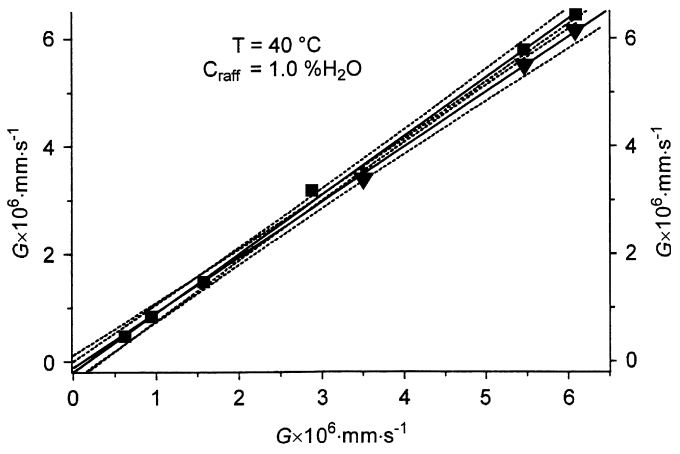

Fig. 5. Comparison between linear overall growth rates determined by three independent ways; in abscissa are represented the values calculated by Eq. (4).

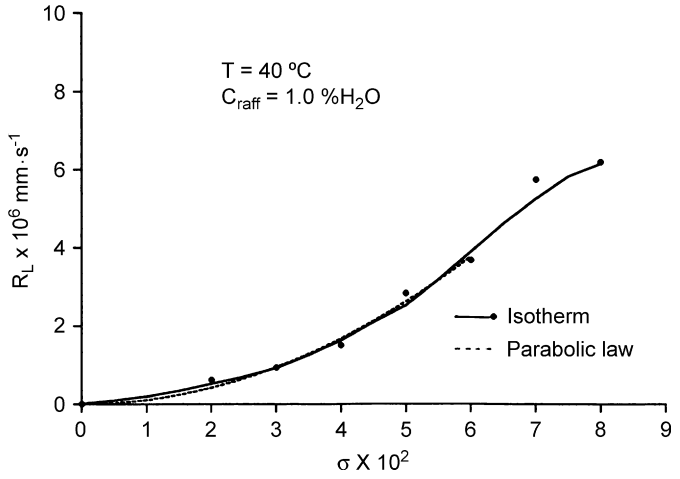

Fig. 6. Growth isotherm of linear overall growth rate of sucrose crystals at $C_{\mathrm{raff}} = 1.0\%$.

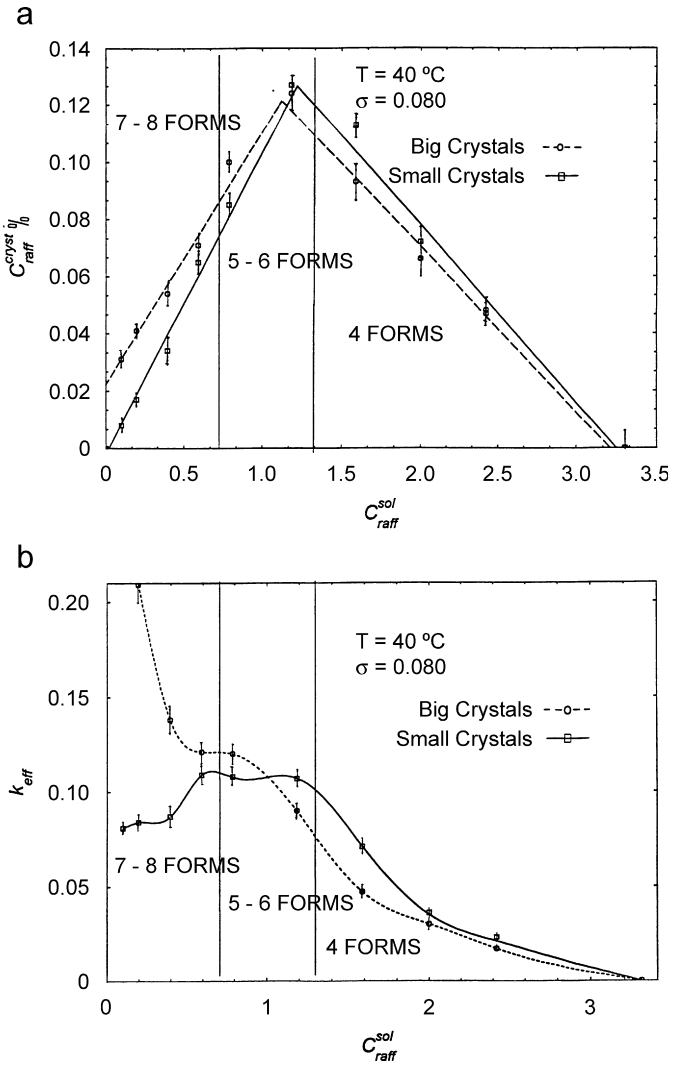

Fig. 7. Dependence on the raffinose concentrations in solution ($C^{\mathrm{sol}}_{\mathrm{raff}}$) of: (a) raffinose concentration in sucrose doped crystals ($C^{\mathrm{cryst}}_{\mathrm{raff}}$) and (b) effective segregation coefficient k_{eff}.

shown to have dubious significance, since other factors make uncertain the measurements [5]. However, the assumption was proved to be acceptable for our aims. The shape of the growth isotherm (G, σ) is parabolic at low σ values, whereas it shows an inflection point at $\sigma \approx 0.06$ (Fig. 6). This clearly rises from the overlapping of the (R_{hkl}, σ) isotherms of the single crystallographic forms [1].

3.3. Segregation

After the study of kinetics, surface adsorption and analysis of the morphology of the doped sucrose crystal, we wondered if and how the growth conditions can affect the incorporation of raffinose into the crystals. Thus, we began with the analysis of its amount inside the crystals, obtained from the two series of small and big seeds during the runs at $\sigma = 0.080$. Then, $C^{\mathrm{cryst}}_{\mathrm{raff}}$ was plotted vs the concentration $C^{\mathrm{sol}}_{\mathrm{raff}}$ in the solution, both $C^{\mathrm{sol}}_{\mathrm{raff}}$ and $C^{\mathrm{cryst/sol}}_{\mathrm{raff}}$ being expressed in g Raffinose/100 g Sucrose (g % S hereinafter) (Fig. 7a). Both curves are not monotonic and can be approximated by two linear parts with opposite slopes, below and above $C^{\mathrm{sol}}_{\mathrm{raff}} \approx 1.6\%$ S $\approx 4\%$ H_2O and vanished at $C^{\mathrm{sol}}_{\mathrm{raff}} \approx 3.3\%$ S $\approx 8\%$ H_2O. Two peculiarities can be pointed out: (a) the extrapolation back to $C^{\mathrm{sol}}_{\mathrm{raff}} = 0$ passes through the origin only for small crystals; and (b) small crystals have a significantly lower raffinose content than the bigger ones below, but similar above the critical value $C^{\mathrm{sol}}_{\mathrm{raff}} = 1.6\%$ S.

Owing to the unusual dependence of $C^{\mathrm{cryst}}_{\mathrm{raff}}$ on $C^{\mathrm{sol}}_{\mathrm{raff}}$, the relationship between the effective segregation coefficient and $C^{\mathrm{sol}}_{\mathrm{raff}}$ was not only complex, but different for the two series of crystals as well (Fig. 7b). The uncertainty of the k_{eff} values reaches near 10% and mainly depends on the dispersion of $C^{\mathrm{cryst}}_{\mathrm{raff}}$ that ranges between 5% and 9%, according to the supersaturation, while the uncertainty of the $C^{\mathrm{sol}}_{\mathrm{raff}}$ values is always lower than 0.05% [1].

The different plots for small and big crystals reveal that the raffinose concentration inside the bigger crystals was

affected by a bias, due to solution inclusions captured when crystals grew over a critical rate. Such a threshold was easily reached by the bigger crystals, which grow faster than the smaller ones [1]. Because we are only dealing with the effective incorporation of the additive in the sucrose lattice, we will only consider small crystals from now on.

Further, we investigated kinetics and mechanism of the raffinose incorporation. Since the literature does not supply any clear definition about the segregation rate of an additive into the host crystals, we proposed a simple rate of raffinose transfer (R_{segr}) based on its mass incorporated into sucrose crystals (m_{raff}) per unit time and surface area given by

$$R_{segr} = \frac{m_{raff}}{A_c t}. \tag{11}$$

Such a rate was found to be 3 order of magnitude lower than the overall growth rate of the sucrose crystal. Rearranging Eq. (11), one can relate R_{segr} to the linear growth rate:

$$R_{segr} = \frac{C_{raff}^{cryst} m_c}{A_c t} = C_{raff}^{cryst} \times R_G = 6\rho_c \left(\frac{\alpha}{\beta}\right) C_{raff}^{cryst} \times G. \tag{12}$$

The (R_{segr} vs G) dependence cannot be linear, for C_{raff}^{cryst} is a function of G. As a matter of fact, the experimental relationship we found reads

$$R_{segr} = (0.633 \pm 0.058) \times 10^{-5} \times G^{(1.24 \pm 0.06)}. \tag{13}$$

Like the growth processes, the segregation of an additive is conditioned either by surface processes involving its adsorption and the subsequent incorporation into the lattice of the host crystal, or by its mass transport by volume diffusion in the boundary layer. Aiming at carrying out a preliminary survey on the segregation mechanism of raffinose, we considered the two classical models proposed by Chernov [3] and Burton–Prim–Slichter [12] (BPS), describing the segregation either dominated by integration processes of the additive on the host crystal faces or by molecular diffusion of the additive within the boundary layer, respectively. From Chernov's model

$$k_{eff} = \frac{k_0}{1 + (\sigma/\sigma^*)}, \tag{14}$$

where k_0 is the equilibrium distribution coefficient, and σ^* some constant depending on the elementary frequencies of attachment and detachment of host and additive particles. σ^* can assume either positive or negative values, according to whether the additive is adsorbed on the crystal faces more ($k_0 > 1$) or less ($k_0 > 1$) than the crystal component. On the contrary, the BPS model which is devised for the melt growth, relates k_{eff} and k_0 through the following expression:

$$k_{eff}^{-1} = \frac{k_0}{k_0 + (1 - k_0)\exp(-\delta G/D)}, \tag{15}$$

where δ and D are parameters related to the diffusion boundary layer thickness and the molecular diffusivity of the additive, respectively. Eq. (15) may also be written in the logarithmic form as

$$\ln(k_{eff}^{-1} - 1) = \ln(k_0^{-1} - 1) - \left(\frac{\delta}{D}\right) G. \tag{16}$$

Hence, to discriminate between these mechanisms, we tested the dependence of k_{eff} on σ, and the relationship between the function $\ln(k_{eff}^{-1} - 1)$ and G, at $C_{raff} = 1.0\%$ H_2O. Thus, the dependence (k_{eff} vs σ) may be represented by the empirical relationship

$$k_{eff} = \frac{0.054 \pm 0.001}{1 - (4.86 \pm 0.171) \times 10^2 \sigma} \quad (r^2 = 0.988). \tag{17}$$

Eq. (16) was given by

$$\ln(k_{eff}^{-1} - 1) = -(0.068 \pm 0.005) \times 10^6 G + (2.77 \pm 0.02) \quad (r^2 = 0.970). \tag{18}$$

Lastly, we also checked the model, proposed by Hall [13],

$$k_{eff} = k_0 \exp\left[\left(\frac{\delta}{D}\right) G\right] \tag{19}$$

that basically is grounded on the same BPS assumption (diffusion within the boundary layer) and can be considered as an approximation of the BPS model (under moderate growth rates and when $k_{eff} \ll 1$). Hall's model, when applied to our data, gives the equation

$$k_{eff} = (0.059 \pm 0.001) \exp[(0.064 \pm 0.005) \times 10^6 G] \quad (r^2 = 0.973). \tag{20}$$

The values of the parameters obtained by applying the two models effectively agreed. Finally, all equations fit good in our data (Fig. 8a and b) and the determination coefficient is high, bearing in mind the dispersion involved in the k_{eff} values.

The quoted data on the raffinose content in the sucrose crystal are global and do not give any information on the anisotropy of the segregation. To highlight this point, we analysed the raffinose concentration in the growth sectors of the two $\{1\,1\,0\}$ and $\{\bar{1}\,\bar{1}\,0\}$ complementary forms.

Fig. 9 shows that the segregation ability of the $\{1\,1\,0\}$ form is almost 1 order of magnitude higher than that of its complementary form, and about twice that of the whole crystal, in agreement with the strong differences found in the surface adsorption on the corresponding forms.

Aiming at attaining further insights into the strains of the host lattice and checking our preliminary results about the anisotropy of the segregation, XRPD patterns were performed on sucrose crystals grown at $\sigma = 0.080$, $C_{raff} = 1.0\%$ H_2O in the range $3^\circ \leqslant 2\theta \leqslant 50^\circ$ (Fig. 10a). Although the diffraction diagrams of doped and undoped sucrose crystals appeared quite similar at a hasty sight, a deeper examination revealed both asymmetry and shoulders in some peak profiles. Actually, the decomposition of the

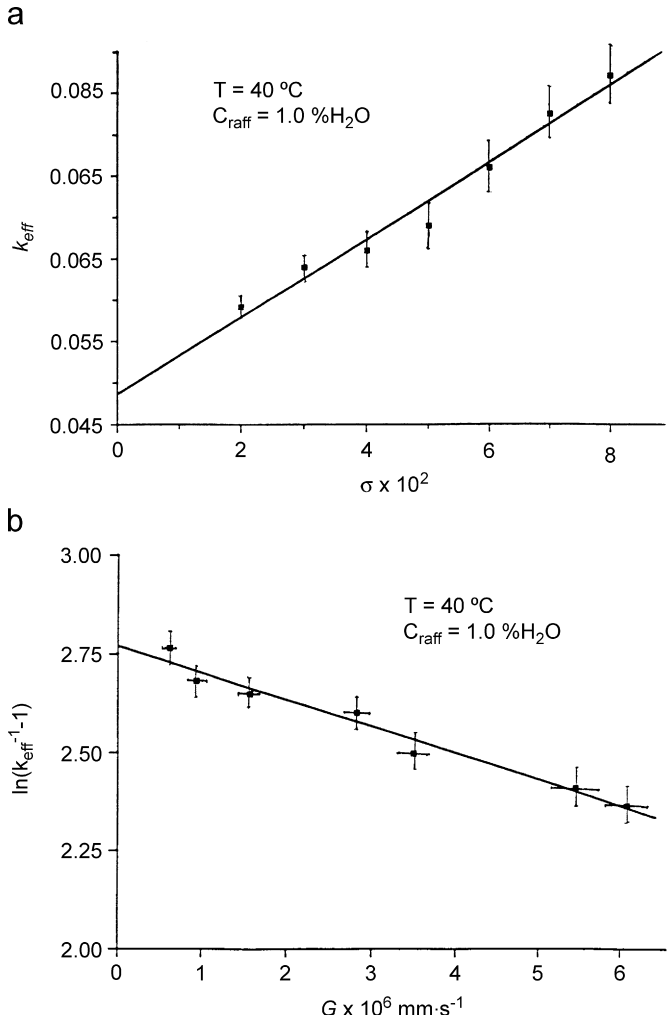

Fig. 8. Fitting of our experimental data to (a) $k_{\text{eff}} = f(\sigma)$ curve (Chernov's segregation model; Eq. (15)) and (b) $\ln(k_{\text{eff}}^{-1} - 1) = f(G)$ curve (BPS's segregation model; Eq. (16)).

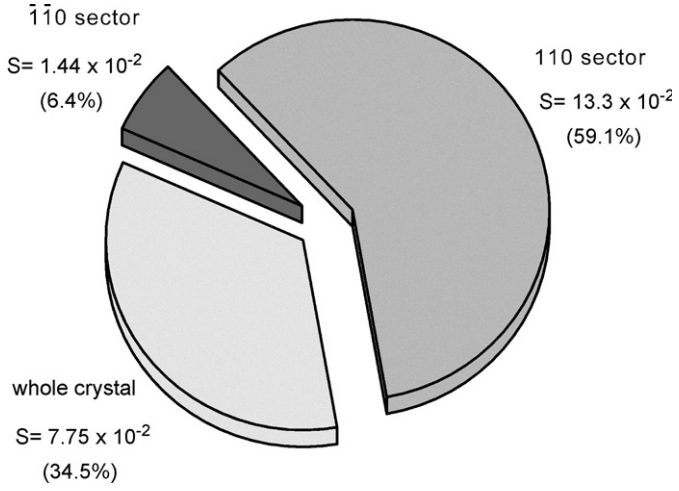

Fig. 9. Distribution of segregated raffinose in the doped sucrose crystals.

pattern peaks in symmetric elementary curves showed two possibilities: the profiles were fitted either by one, or by more (two or even three) elementary components (Fig. 10b).

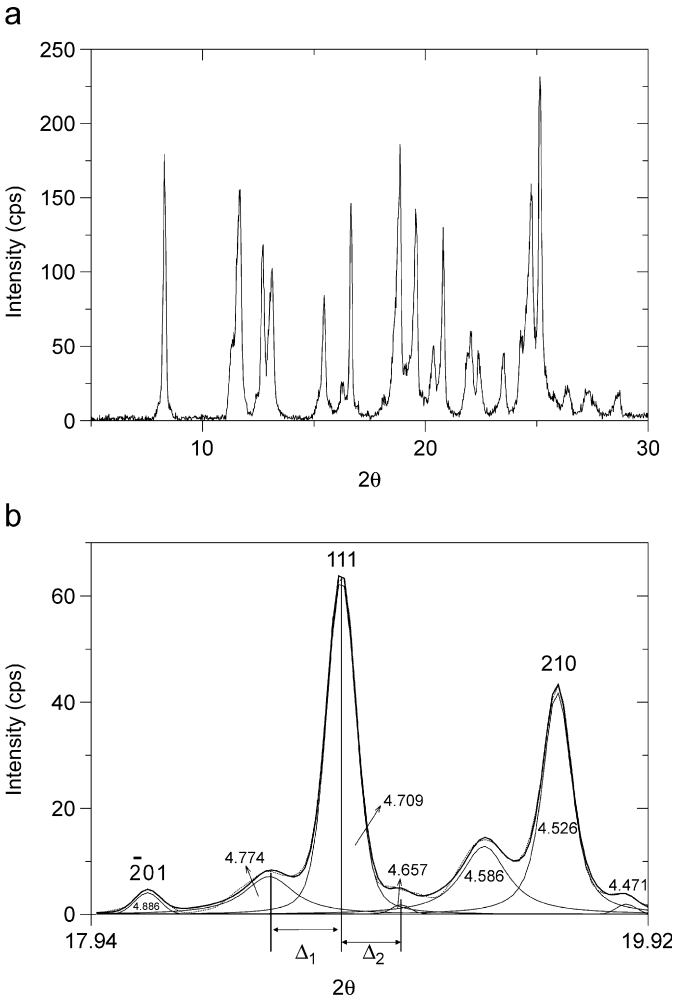

Fig. 10. (a) XRPD pattern of sucrose crystals grown at $\sigma = 0.080$ in the presence of $C_{\text{raff}} = 1.0\%$ H_2O and (b) decomposition of $\bar{2}01$, 111 and 210 peaks.

4. Discussion

4.1. Morphology

The morphodrome clearly shows that supersaturation and raffinose concentration produced conflicting effects. Anyway, the strong additive effect caused the simplest morphology to be by far dominant in the (C_{raff}, σ) plane, but for the highest σ values. Another important feature characterizes the non-polar $\{h\,0\,l\}$ zone: even if raffinose had no influence on the growth rate of the $\{1\,0\,1\}$ form [6], its importance strongly affected the crystal shapes obtained up to $C_{\text{raff}} = 0.5\%$ H_2O, in particular in the third zone of the morphodrome. This suggests the prevailing effect of σ over the additive: the non-polar zone looks like that of crystals growing in pure solutions. Once more, the peculiar S→F character transition of the $\{1\,0\,1\}$ form can be recollected [14]. Thus, the water molecules clamping the PBC's $[0\,1\,0]$ within the d_{101} slices probably masked the feeble growth slowing down induced by raffinose on the adjacent $\{0\,0\,1\}$ form.

The different pattern of $\varepsilon(C_{raff})$ and $\delta(C_{raff})$ curves (Fig. 3) is a consequence of the kind of measured lengths. In fact a', the distance between the faces of the $\{1\,0\,0\}$ pinacoid, and b, the distance between the $[0\,0\,1]$ edges of the $\{1\,1\,0\}$ and $\{\bar{1}\,\bar{1}\,0\}$ sphenoides, are proportional to the growth time ($2R_{100}$ and $(\cos 39.38^\circ)^{-1} \times (R_{110} + R_{\bar{1}\bar{1}0})$ being the respective constants under steady growth). Thus,

$$\varepsilon = \frac{(a_0 + 2R_{100} \times t)}{b_0 + (R_{110} + R_{\bar{1}\bar{1}0}) \times (\cos\ 39.38^\circ)^{-1} \times t}, \tag{21}$$

where a_0 and b_0 are the initial seed dimensions, 39.38° is the half of the angle between the sphenoid faces and t is the growth time. The differences between measured and calculated ε, δ ratios are $\leqslant 5\%$. The calculated ε value can be estimated as well from the steady growth shapes of the crystals (Fig. 4)

$$\lim_{t\to\infty} \varepsilon = \frac{2R_{100}}{(R_{110} + R_{\bar{1}\bar{1}0}) \times (\cos\ 39.38^\circ)^{-1}}. \tag{22}$$

On the contrary, c, the distance between the farthest two $[0\,1\,0]$ crystal edges, was not proportional to the growth time because its increase was not steady, due to the morphological changes in the $\{h\,0\,l\}$ zone. In fact, the position of the $[0\,1\,0]$ edges was influenced by the fast extension changes of the areas of $\{1\,0\,1\}$ and $\{0\,0\,1\}$ forms during growth. This is the reason why it is not possible to calculate the ratio δ using a formula similar to Eq. (21) and the growth rates measured *ex situ*. Only when those forms disappeared from the morphology, that is, when the crystals were bounded by four forms, the growth in the $\{h\,0\,l\}$ zone became steady: thus, ε and δ theoretical ratios tend to the same value, since both R_{100} and $R_{10\bar{1}}$ nearly vanished. Until this condition was not fulfilled, c increased more than b and then maxima appeared on $\delta(C_{raff})$ curves.

We already pointed out that both ε and δ values calculated by means either of the steady shapes or of relation (22) agreed with the experimental ones up to $C_{raff} \approx 3\%$ and 1%, for 0.080 and $\sigma = 0.040$, respectively. On the contrary, gaps occurred at higher concentrations, as in pure solution (Fig. 3). This suggests that the ε and δ ratios reasonably estimated the growth morphology only within the range of the low additive concentrations. The gaps arose from the too short growth runs, which are needed in order that shapes and sizes of the grown crystals should not be influenced by the initial morphology of the seeds. Concerning the ε ratio, the dominant supersaturation effect reflects on the numerator and denominator changes (see relation (22)) in about the same extent obtained with low C_{raff}, so that ε remained nearly constant. At higher concentrations, ε value decreased because only the denominator increased, due to small slowing down of the $R_{\bar{1}\bar{1}0}$, and to the conditions: $R_{100} \ll 1$, $R_{110} \approx 0$. Hence, the monotonically decreasing pattern of $\varepsilon(C_{raff})$ curves appears to be justified.

4.2. Segregation

We have not been able to notice in the literature any system showing a non-monotonic dependence of k_{eff} on C^{sol}_{raff}. However, the peculiar behaviour, we found in the case of the raffinose segregation, suggests a close correlation between segregation and changes of growth morphology. In fact, the raffinose content in the crystals increased up to the critical value $C^{sol}_{raff} \approx 1.6\%S \approx 4\%\ H_2O$, that is, as long as the more the affected forms $\{1\,1\,0\}$, $\{1\,0\,\bar{1}\}$ and $\{1\,0\,0\}$ grew at detectable rate. Over this threshold value, only the $\{1\,0\,0\}$ form can grow at a significant rate; moreover, the $\{\bar{1}\,\bar{1}\,0\}$ form was also slowed down, in spite of its poor adsorption ability. Crystals got the simplest growth morphology, and the segregation rate became always lower (Eq. (13)), up to vanishing at $C^{sol}_{raff} \approx 3.3\%\ S \approx 8\%\ H_2O$. After all, a volume process as the raffinose absorption was then reduced to a pure surface adsorption: the amount of raffinose adsorbed only at the surfaces of the host crystals was too low to be detected!

The linear increase of C^{cryst}_{raff} also states that the energy of the elastic deformation of the host lattice sectors getting involved in the segregation was weak, at least up to the critical threshold. The segregation rate cannot be proportional to R_G (or G) (Eq. (13)), because the raffinose concentration in turn depended on them. However, a linear dependence can be admitted, in the first approximation.

Concerning the segregation mechanism, it is worth to reaffirm that

(i) the present survey is nothing else that a first approach to the evaluation of the averaged behaviour of the raffinose uptake in the sucrose crystal; and
(ii) we did not take into account the sectorial segregation that witnesses the strong dependence of the impurity uptake on the crystallographic orientation.

Reviewing Eqs. (16), (17), and (20) in the light of these considerations, one can say that their good linear trend could satisfactorily predict the behaviour of k_{eff} as a function of either σ or G and then that they cannot be used in distinguishing the segregation mechanism.

Moreover, it should be mentioned that the equilibrium distribution coefficients k_0 calculated from Chernov's, BPS's and Hall's models hold 0.054, 0.059 and 0.059, respectively. These very close values, all being $\ll 1$, confirm that raffinose molecules are more weakly adsorbed than those of sucrose during the growth process [3]. This fully agrees with the behaviour of all sucrose $\{h\,k\,l\}$ forms but the $\{1\,0\,\bar{1}\}$ [14–17].

Nevertheless, to validate the models it is necessary to verify the effective physical consistency of parameters. But, unfortunately, any experimental data are available neither on the adsorption and de-adsorption frequencies of sucrose and raffinose (from which depends the σ^* parameter in the Chernov's model) nor on δ and D values which are shared by BPS's and Hall's models.

However, one can try to estimate the boundary layer thickness through the well-know relation [18]

$$\delta = \left[\frac{2}{3}\left(\frac{\eta}{\rho D}\right)^{1/3}\left(\frac{\rho u}{\eta L}\right)^{1/2}\right]^{-1}, \quad (23)$$

where (η/ρ) represents the kinematic viscosity and u is the relative crystal/solution velocity. Reasonably assuming that $C_{raff} = 1\%$ H_2O does not affect the value of the kinematic viscosity of pure sucrose solutions (71 wt% at 40 °C), we supposed $(\eta/\rho) = 106 \times 10^{-6}\,mm^2\,s^{-1}$ [19], $u = 10\,mm\,s^{-1}$ and $L = 2\,mm$, and found $\delta = 5.8 \times 10^{-2}\,mm$ that is consistent with $\delta = 0.17\,mm$ we measured at room temperature in static solutions (72% sucrose in weight) [20]. From the mean slope (0.066×10^6) of the straights (Eqs. (18) and (20)), we estimated the diffusion coefficient $D_{raff} = 8.8 \times 10^{-7}\,mm^2\,s^{-1}$ that is nearly 1/60 of $D_{sacc} = 53.2 \times 10^{-6}\,mm^2\,s^{-1}$ [19]. This seems to be very reasonable, owing to the fact that the raffinose molecule is larger than that of saccarose and coordinates a larger number of water molecules (the crystalline raffinose is hexahydrated), both factors hindering the diffusive transport.

Starting from these considerations and taking into account the agreement of the parametric values in Eqs. (18) and (20), we could venture the guess that the raffinose incorporation is determined either by a BPS or, by the more simply Hall diffusive mechanism that can be favoured by the supersaturated sucrose solutions which could be assimilated to the melts. On the other hand, two factors should give some evidence in Chernov's model favour

- the strong anisotropy of the raffinose segregation that witnesses for the relevance of surface structure of the different crystallographic forms; and
- the discontinuity of the raffinose concentration in the crystal (as a function of its concentration in solution) which might be the consequence of the competition between the two adsorbed species.

Summing up, our experiments are not able, at the time being, to clarify what is the mechanism prevailing in the complex segregation processes of raffinose. When extending the growth runs to the solutions with higher raffinose concentrations, a more complete picture will be given and then the experimental data will be examined in the light of more recent models that take into account also the supersaturation barriers observed in the presence of impurities [21].

The profiles of the modified peaks of the XRPD patterns, corresponding to the expected d_{hkl} values, can be fitted by three elementary curves, the central of which refers to the diffraction from the pure crystal (unperturbed lattice domains and initial seed), and the two others $(d_{hkl}+\Delta_1)$ and $(d_{hkl}-\Delta_2)$ to the diffraction from the d_{hkl} equidistances deformed by the raffinose inclusion within the corresponding growth sectors.

An unambiguous example of peak splitting is offered in Fig. 10b, showing a short diffraction range $(17.940° \leqslant 2\theta \leqslant 19.920°)$, which is representative of the entire pattern. As a matter of fact, the $\bar{2}10$ peak, whose growth sector does not segregate, can be perfectly fitted by only one elementary curve, whilst the perturbed 111 and 210 peaks can be decomposed in three functions. The different profiles of the 210 and $\bar{2}10$ peaks, even if produced by minor growth sectors, clearly illustrate the different segregation ability of the complementary forms. The volume changes of the perturbed elementary cells were not homogeneous with respect to the size of their sides, which excludes absorption of the raffinose as a component of a solid solution (Vegard law does not hold). Summing up, the above evidences confirm that the raffinose segregation is highly anisotropic in doped sucrose crystals. Moreover, three fractions of the lattice equidistances can picked out: one unperturbed, at d_{hkl}, one "swelled" at $(d_{hkl}-\Delta_1)$ and the last "compressed" at $(d_{hkl}+\Delta_2)$, probably due to a long-range effect.

5. Conclusions

From the present study, we can infer the following conclusions:

- (C_{raff}, σ) morphodromes well represent the conflicting effects produced by supersaturation and raffinose concentration on the growth morphology of sucrose crystals (Fig. 2).
- Quantitative experimental morphologies (ε and δ ratios), satisfactorily estimate the steady growth morphologies when the overall growth rate is high, namely only at low C_{raff} (Fig. 3).
- There is a correlation between growth morphology and raffinose absorbed in sucrose crystals: its content (at $\sigma = 0.080$) increases up to $C_{raff} \approx 4\%$ H_2O, and decreases over this critical value, when the morphology reduces to only four forms (Fig. 5).
- The overall segregation rate is nearly proportional to the linear overall growth rate G (Eq. (13)).
- Chernov's, BPS's and Hall's models well fit our k_{eff} and $\ln(k_{eff}^{-1} - 1)$ as a function of σ and G, respectively (Fig. 8a–c). This does not allow to distinguish whether the segregation occurs either by a process controlled by surface integration, or by additive transfer dominated by volume diffusion within the boundary layer. However, the equilibrium distribution coefficient k_0, calculated from the models ranges from 5.4×10^{-2} to 5.9×10^{-2}. Furthermore, from the BPS's and Hall's models, the value of the diffusion coefficient of the raffinose has been estimated to be $D_{raff} = 8.8 \times 10^{-7}\,mm^2\,s^{-1}$, that seems to be reasonable with respect to that of sucrose, at the same supersaturation value.
- The distribution of segregated raffinose is not uniform inside the sucrose crystals, strictly depending on the

$\{h\,k\,l\}$ growth sectors, in agreement with the adsorption ability of the corresponding faces (Fig. 9).

- Doped crystals contain deformed lattice zones, whose elementary cell volume can be either larger or smaller than that of the pure sucrose lattice. However, the consequent elastic reactions are too weak to withstand regular additive incorporation, at least up to the critical value $C_{\mathrm{raff}}^{\mathrm{cryst}} \approx 11.3 \times 10^{-2}\%$ S. An exhaustive description of the growth process of sucrose crystals in the presence of raffinose yet needs further experiments, some of which are in progress in our laboratories.

References

[1] G. Sgualdino, D. Aquilano, A. Cincotti, L. Pastero, G. Vaccari, J. Crystal Growth 292 (2006) 92.
[2] (a) N. Kubota, J.W. Mullin, J. Crystal Growth 152 (1995) 203;
(b) N. Kubota, N. Yokota, J.W. Mullin, J. Crystal Growth 182 (1997) 86.
[3] A.A. Chernov, in: A.A. Chernov (Ed.), Modern Crystallography III: Crystal Growth, Springer, Berlin, 1983 (Chapter 4).
[4] A. Van Hook, H. Beall, Proc. Res. Soc. (Japan Sugar Refineries' Technologists) 26 (1976) 74.
[5] F. Schneider, A. Emmerich, O.Ç. Akyar, Zucker 28 (1975) 113.
[6] G. Vaccari, G. Mantovani, G. Sgualdino, D. Aquilano, M. Rubbo, Sugar Technol. Rev. 13 (1986) 133.
[7] G. Sgualdino, D. Aquilano, R. Fioravanti, G. Vaccari, L. Pastero, Cryst. Res. Technol. 40 (2005) 1087.
[8] R. Kern, in: I. Sunagawa (Ed.), Morphology of Crystals (Part A), Terra Scientific Publishing Company, Tokyo, 1987 (Chapter 2).
[9] SHAPE for Window, Version 6.0.1, professional ed., Copyright 2000 by E. Dowty.
[10] Z. Bubník, P. Kadlec, Zuckerind 117 (1992) 345.
[11] J.W. Mullin, Crystallization, Butterworth-Heinemann Ltd., Oxford, 1993 (Chapter 6).
[12] J.A. Burton, R.C. Prim, W.P. Slichter, J. Chem. Phys. 21 (1953) 1987.
[13] R.N. Hall, J. Phys. Chem. 57 (1953) 836.
[14] D. Aquilano, M. Rubbo, G. Vaccari, G. Mantovani, G. Sgualdino, in: S.J. Jančić, E.J. de Jong (Eds.), Industrial Crystallization, vol. 84, Elsevier, Amsterdam, 1984, p. 91.
[15] D. Aquilano, M. Rubbo, G. Mantovani, G. Vaccari, G. Sgualdino, in: A.S. Myerson, K. Toyokura (Eds.), Crystallization as Separation Process, ACS Symposium Series, Washington, DC, 1999, p. 72.
[16] G. Vaccari, G. Mantovani, G. Sgualdino, D. Aquilano, M. Rubbo, Sugar Technol. Rev. 13 (1986) 133.
[17] C. Campaña Cuè, A.R. Ruiz Salvador, S. Aguilera Morales, F.L. Falcon Rodriguez, P. Pérez Gonzàlez, J. Crystal Growth 231 (2001) 280.
[18] P. Bennema, J. Crystal Growth 3 (4) (1968) 331.
[19] Z. Bubnik, P. Kadlec, D. Urban, M. Bruns, Sugar Technologists Manual, eighth ed., Bartens, Berlin, 1995.
[20] F. Bedarida, L. Zefiro, P. Boccacci, D. Aquilano, M. Rubbo, G. Vaccari, G. Mantovani, G. Sgualdino, J. Crystal Growth 89 (1988) 395.
[21] K. Sangwal, T. Palczynska, J. Crystal Growth 212 (2000) 522;
K. Sangwal, J. Crystal Growth 242 (2002) 215.